RSC Advances

ROYAL SOCIETY OF CHEMISTRY

www.rsc.org/advances

A promising photoelectrochemical sensor based on a ZnO particle decorated N-doped reduced graphene oxide modified electrode for simultaneous determination of catechol and hydroquinone

A.T. Ezhil Vilian[a], Muniyandi Rajkumar [b], Shen-Ming Chen[a]* Chi-Chang Hu [b], Shakkthivel Piraman [c],

[a]*Department of Chemical Engineering and Biotechnology, National Taipei University of Technology, No.1, Section 3, Chung-Hsiao East Road, Taipei 106, Taiwan (R.O.C).

[b] Laboratory of Electrochemistry & Advanced Materials, Department of Chemical Engineering, National Tsing Hua University, Hsinchu 30013, Taiwan (R.O.C).

[c] Sustainable and Smart Materials Research Lab., Department of Nano Science and Technology, Alagappa University, Karaikudi 630 002, Tamil Nadu, India

*Corresponding author. Fax: +886 2270 25238; Tel: +886 2270 17147,
E-mail: smchen78@ms15.hinet.net

Abstract

This paper describes the synthesis of Nitrogen-doped reduced graphene oxide ZnO (N-doped RGO-ZnO) nanocomposite by two-step process and also its photo electrochemical application. The novel photo electrochemical sensor fabricated from this ZnO/N-doped RGO nanocomposite exhibits superior performance over a glassy carbon or nitrogen-doped reduced GO nanocomposite for the simultaneous determination of hydroquinone (HQ) and catechol (CC). Cyclic voltammetry (CV) studies reveals that the N-doped RGO-ZnO electrode under optimal conditions show a peak potential separation between HQ and CC of up to 112 mV in the presence of light, which is larger than N-doped RGO electrode under same condition. Square wave voltammetry (SWV) studies of a system with co-existing HQ and CC show that the N-doped RGO-ZnO modified electrode exhibits a wide linear response range of 2-900 μM and 2-600 μM, respectively, with detection limits (S/N=3) of 10 nM and 10 nM, respectively. The electrode also has good sensitivity, selectivity, high stability and reproducibility. This electrode sensor was further applied to determine HQ and CC in real samples with satisfactory results. The results demonstrate that the N-doped RGO-ZnO is a more robust and advanced carbon electrode material providing a promising platform for photo electrochemical sensor and photo electrocatalytic applications.

Keywords: photo electrochemical sensors, reduced graphene oxide, hydroquinone and catechol, ZnO nano particles.

1. Introduction

In recent years, photo electrochemical (PEC) biosensing has emerged as a new analytical scientific and technological technique for the production of sensing platforms, in which light is utilized to excite the photoactive species and the photocurrent is employed as the detection signal.[1-4] PEC sensors are receiving increasing attention owing to their desirable high sensitivity, fast response time, low cost, inherent miniaturization, portability and easy integration.[5-8] These advantages have brought a wide range of prospective applications in the fields of biology, medicine, and environmental monitoring.[9-11]

Graphene, a single layer of carbon atoms with a honeycomb-like two-dimensional lattice has become a rising star in the carbon family due to its novel properties such as high surface area, good electrical conductivity, high flexibility and mechanical strength since its discovery in 2004.[12-14] In recent years, it has attracted considerable attention in both fundamental science and in experimental and applied research areas in many fields, such as in nanoelectronics,[15,16] ultra capacitors,[17] batteries,[18] sensors,[19,20] solar cells,[21] and fuel cells.[22, 23]

In the past few years, some photo electrochemical materials such as TiO_2,[24] ZnO,[25]and quantum dots have been employed for PEC sensing. [26] ZnO is an important semiconductor nonmaterial, used in the field of photo electrochemical sensing due to its desirable qualities, such as photosensitivity, chemical stability, environmental friendliness, and better analytical performance.[27] Zinc oxide nanoparticles are a promising semiconducting material for use in solar cells, having a wide band gap of 3.37 eV and a large exciton binding energy of 60 meV at room temperature as well as excellent chemical, and structural features.[28-31] Zinc oxide is one of the most commonly used photo catalyst materials for purposes such as the degradation of organic

pollutants under UV-light, sometimes demonstrating a higher photo catalytic activity than TiO_2.[32-34]

Very recently, the practical application of graphene for the electrochemical sensing of biomaterials has been heavily researched.[35] Graphene acts as an excellent electron-acceptor/transport material facilitating the process of photo catalysis. The electronic interaction between ZnO and graphene can hinder the recombination of charge carries and increase the photo catalytic performance.[36-37] In the past few years, a variety of methods have been used for the fabrication of graphene/ZnO nanocomposites. The photoluminescent (PL) characteristics of vertically-grown ZnO nanostructures synthesized by catalyst-free metal-organic vapor-phase epitaxy on graphene layers has been examined. [38] Wu *et al*. used a solvothermal method to prepare a sandwich-like graphene-ZnO nanocomposite in an ethylene glycol medium with graphene oxide (GO) as the graphene precursor and zinc acetylacetonate as the single-source zinc oxide precursor. [39] Lu *et al.* reported on the development of graphene-ZnO nanocomposite films by ultrasonic spray pyrolysis.[40] Li *et al*. produced a ZnO/graphene nanocomposite using a chemical decomposition method. [41] However, to the best of our knowledge, there are no reports available in the literature for the synthesis of ZnO on an N-doped-RGO surface.

Hydroquinone (HQ) and catechol (CC) chemically known as (1,4 dihydroxybenzene), catechol (1,2- dihydroxybenzene) are two isomers of phenolic compounds which are widely used in the production of cosmetics, pesticides, flavoring agents, medicines, food, dye stuffs, photographic chemicals and so on.[42-45] These phenolic compounds are highly toxic to human beings, animals, and plants and damaging to aquatic environments, even at very low concentrations.[46,47] They are suspected of being carcinogens and their degradation has a negative

impact on the environment. It is known that an abnormal phenolic compound level can lead to fatigue, headache and tachycardia in humans and cause kidney damage. [48]

It is thus necessary to establish a simple, fast and reliable analytical method for the sensitive and selective determination of HQ and CC in various matrices. [49] Several analytical methods have been employed to evaluate these isomers such as high performance liquid chromatography, pH based-flow injection analysis, synchronous fluorescence, chemiluminescence, spectrophotometry, gas chromatography and mass spectrometry, capillary electro chromatography and electrochemical methods.[50,51] However, some of these methods can be time-consuming, high cost, with low sensitivity and requiring complicated pretreatment. Photo electrochemical methods are the most commonly used techniques in environmental and biological research because of their high sensitivity, rapid response time, low detection limit and ease of operation.

The HQ and CC isomers are similar in structure and properties and usually coexist, thus interfering with each other during identification. It is necessary to develop an effective photo electrochemical sensor for the simultaneous detection of HQ and CC which are both electrochemically active.

To the best of our knowledge, this is the first time that the use of ZnO/N-doped RGO nanocomposites for the simultaneous determination of HQ and CC has been reported. This novel approach allows simultaneous detection of HQ and CC in a solution through a photo electrochemical method such as cyclic voltammetry (CV) or square wave voltammetry (SWV). The morphology and structure of the synthesized N-doped RGO-ZnO nanocomposites were investigated in detail by scanning electron microscopy (SEM), X-ray diffraction (XRD), X-ray

photoelectron spectroscopy (XPS) and Raman spectroscopy. The N-doped RGO-ZnO nanocomposite was then used to fabricate a novel photo electrochemical sensor for the detection of HQ and CC. This material provided a larger electrochemically active surface area for the adsorption of HQ and CC that effectively accelerated the electron transfer between the electrode and the solution, which could lead to a more rapid and sensitive current response. It is well known that the photo electrochemical method is a very tedious, time-consuming and high cost process making the development of a less expensive method with a simple fabrication procedure desirable. The device was used for simultaneous detection of HQ and CC in real samples of skin whitening cream and lake water.

2. Experimental Procedure

2.1. Reagents and materials

Graphite (powdered, <20 μm), N,N-dimethylformamide (DMF), $Zn(NO_3)_2$, $KMnO_4$, catechol, (CC) and 1, 4-dihydroxyquinone (HQ) were obtained from Sigma-Aldrich and used without further purification. With the aid of ultrasonic mixing, 0.10 M stock solutions with HQ or CC were freshly prepared by dissolving HQ or CC in 0.05 M pH 7 PBS buffered solutions which were kept at 4°C in the dark prior to use. The stock solution was diluted to various concentrations by mixing with the buffer solution. Double distilled water (with a resistivity of 18.25 MΩ cm) was used throughout. All other materials used were of the highest analytical grad available and purchased from the usual sources. Phosphate buffered solutions (PBS) (pH 7.0) were prepared using 0.05 M Na_2HPO_4/NaH_2PO_4, and 0.1 M KCl.

2.2. Apparatus

Electrochemical measurements were carried out at a CH Instrument 405A electrochemical workstation (Shanghai Chen Hua Co., China). The conventional three-electrode

system included either a bare Au electrode (Φ = 3 mm) or N-doped RGO-ZnO nanocomposite modified Au electrode as the working electrode, a platinum wire as the auxiliary electrode, and an Ag/AgCl (saturated KCl) as the reference electrode. SEM images were made with a Hitachi S-3000 H and EDX images were recorded using a HORIBA EMAX X-ACT Model 51-ADD0009. Transmission electron microscopy (TEM) images were collected using a Philips TECNAI 20 microscope (200 kV). EIS was carried out at a frequency range of 100 kHz to 1.0 Hz with a ZAHNER instrument (Kroanch, Germany) with a controlled intensity modulated photo spectroscopy (CIMPS) system used for light induced EIS and photoelectrocatalytic studies. The PEC and sensing measurements were carried out on a CHI405A electrochemical workstation. The simulated solar light was generated by a KEITHLEY 2400 solar simulator with a 150 W xenon lamp and an AM 1.5G filter. XPS analysis was carried out using a PHI 5000 Versa Probe equipped with an Al Kalpha X-ray source (1486.6 eV). Raman spectra were measured with a Raman spectrometer (Dong Woo 500i, Korea) equipped with a charge-coupled detector. Fourier transform infrared (FTIR) spectra were obtained using a Perkin Elmer RXI spectrometer. XRD analysis was carried out using an XPERT-PRO diffractometer (PANalytical B.V., the Netherlands) using Cu Kα radiation (k =1. 54 A◦).

2.3. Procedures

2.3.1. Synthesis of graphene oxide

The GO used in the experiments was synthesized from natural flake graphite powder by the modified Hummers method described previously.[52] Briefly, graphite powder (5.0 g) was put into 0 °C concentrated H_2SO_4 (150 mL) and then 25 g of $KMnO_4$ was slowly added under ice cooling. The mixture was stirred continuously for 30 min. Typically, 600 mL of deionized water

was added while the temperature was kept under 50 °C, 250 ml of water and 6 ml of H_2O_2 (30 weight %) were subsequently added to reduce the residual $KMnO_4$. The reaction was allowed to continue for 30 min, yielding a brilliant yellow solution. Finally, the solid suspension was first washed using 2 M of HCl solution and then washed 3-4 times with ethanol and dried overnight in a vacuum at 60 °C. The reduced graphene oxide slurry was then dried in a vacuum oven at 60 °C for 48 h before use. A 1:10 mass ratio of the reduced graphene oxide and melamine mixture was transferred into a corundum tube prior to annealing at 800 °C for 1 hour in the presence of a N_2 atmosphere. After annealing, the corundum tube was taken out of the muffle furnace and allowed to cool down to room temperature.

The melamine provided a positively charged layer, which attracted the negatively charged reduced GO (RGO) through electrostatic interaction. The final product of reduced graphene oxide and melamine was obtained. Then, graphene oxide/melamine nanocomposites and ZnO sample were prepared as follows: after one hour of ultrasonic treatment the 0.0904 g/100 mL GO formed a light-brown solution. The obtained exfoliated RGO was then dispersed in 50 mL of water and dropped into an aqueous $Zn(NO_3)_2$ solution with continuous stirring for 24 h. Afterward, 1 M of the KOH solution was added drop by drop into the above mixture until the pH rise to 8.5. After aging for 12 h, the N-doped RGO-ZnO nanocomposite precursors were then filtered and washed with a large amount of distilled water several times before being dried at 60 °C for 24 h under a vacuum. Furthermore, the N-doped RGO-ZnO nanocomposite precursors were heated at 200 ºC for 5 h in a muffle furnace to obtain the resultant product. The N-doped RGO-ZnO nanocomposite sample was prepared by dispersing 0.5mg mL^{-1} of the N-doped RGO-ZnO nanocomposite in 1DMF with the aid of ultrasonication for 30 minutes.

2.3.2. Preparation of the N-doped RGO-ZnO nanocomposite modified Au electrode

Prior to use, the Au electrode (diameter = 3 mm) was carefully polished to a mirror-like plane with 0.05 mm alumina slurries using a Buehler polishing kit. Afterward, the electrode was washed with 1:1 nitric acid, absolute ethanol and water in an ultrasonic bath under nitrogen gas. The synthesized N-doped RGO-ZnO nanocomposite (0.5mg) was dissolved in 1 mL DMF through ultra-sonication for 20 min, resulting in a uniform black solution. 5μL of the N-doped RGO-ZnO nanocomposite suspension was dropped on the surface of the cleaned Au electrode and dried under an infrared lamp. The modified Au electrode was then rinsed with water to remove any loosely adsorbed N-doped RGO-ZnO nanocomposite, higher amounts of which could agglomerate on the electrode surface, affecting the catalytic activity and stability. For comparison, an N-doped RGO nanocomposite was fabricated following similar procedures. A schematic representation showing the step-wise fabrication process of the N-doped RGO-ZnO nanocomposite is provided in scheme 1.

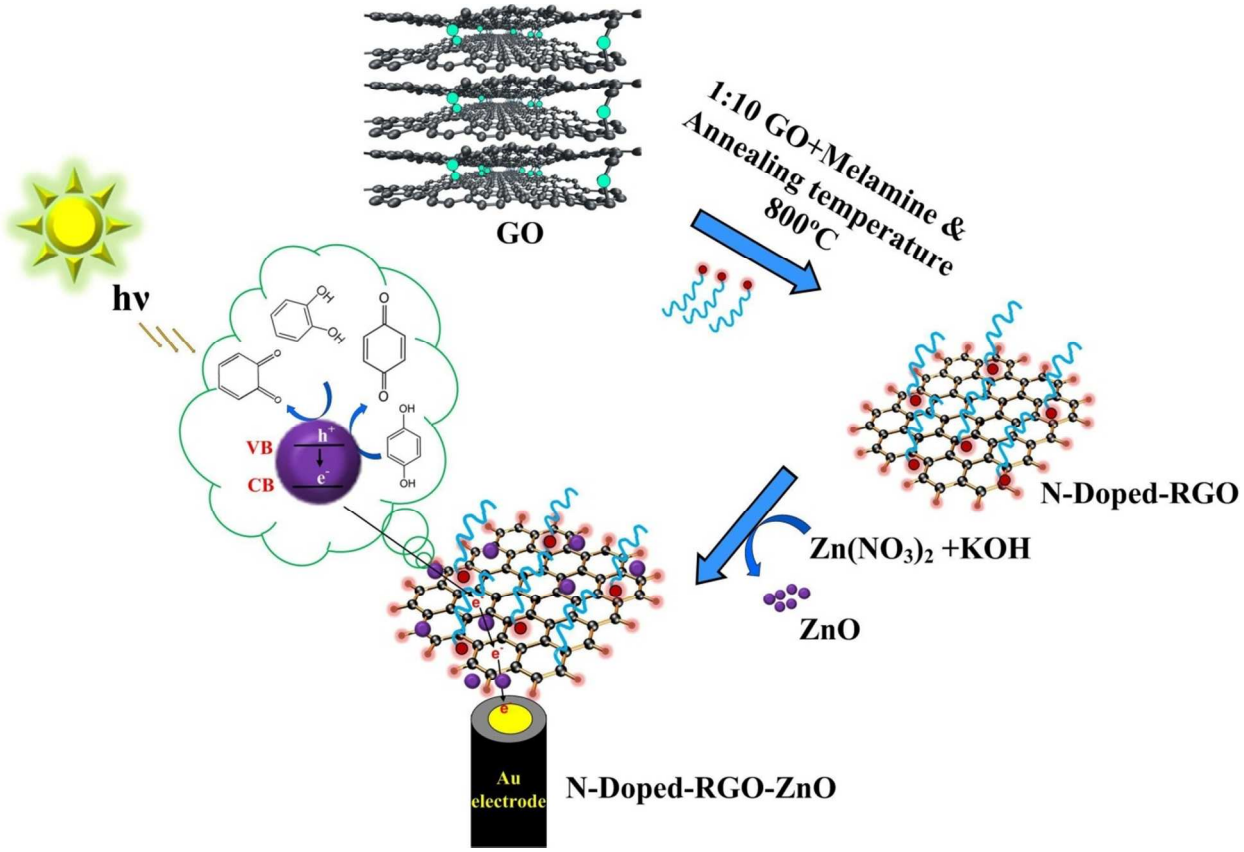

Schematic view of the procedure for preparing the N-doped RGO-ZnO nanocomposite modified electrode.

3. Results and discussion

3.1. Characterization of the N-doped RGO-ZnO nanocomposite

Fig. 1 shows the typical XPS spectra obtained for the N-doped RGO-ZnO nanocomposite and the deconvolution analysis of the Zn 2p, N 1s, C1s and O 1s core level spectra. The XPS spectrum in Fig. 1A displays five predominant peaks, namely the Zn $2p_{3/2}$ peak at around 1021.5 eV, the C 1s peak at around 284.7 eV, the Zn $2p_{1/2}$ peak at around 1046.0 eV, the N 1s peak at around 399 eV, and the O 1s peak at around 532.6 eV. As shown in Fig. 1D, there is a reasonable fit between the N 1s XPS spectrum for the N-doped RGO-ZnO nanocomposite with

three components: pyridine type N at 398.3 eV, amino type N at 399.4 eV and graphitic type N at 401.1 eV. The results suggest that the amino type N atoms have been successfully incorporated into the graphene framework and exist as three kinds of chemical states in the graphene layers. Meanwhile the oxygen-containing functional groups could be removed during the N-doping process. The Zn $2p_{3/2}$ and Zn $2p_{1/2}$ (with binding energies of 1021.5 eV and 1046.0 eV, respectively; See Fig. 1E) [41] as illustrated in Fig. 1E further confirm the formation of ZnO. The C 1s spectrum shows a significant decrease in the C=O components relative to C-C, as depicted in Fig. 1B. This result suggests that the oxygen containing groups have been removed by the Zn^{2+} ions, which proves that the Zn^{2+} ions resulted in the deoxygenation process of GO. In Fig. 1C one can see an obvious peak shift of approximately 529.8 eV for the O 1s spectrum of the N-doped RGO-ZnO nanocomposite, which can be attributed to the O ions in the ZnO lattice, compared to that of GO, which is due to the existence of O^{2-} species in the graphene nanocomposite.[53]

An FTIR study was carried out to verify the presence of oxygen-containing functional groups on the GO sheets which can generate strong interactions with the melamine matrix mainly by amide linkage. As shown in Fig.1F (Curve a), the exfoliated GO sheet exhibits three characteristic peaks, -OH (~3450 cm^{-1}), C=C (~1594 cm^{-1}), C-OH (1216 cm^{-1}), and carbonyl (~1720 cm^{-1}) peaks, which confirm the formation of the carboxyl and hydroxyl groups, respectively. The peaks at 1639 cm^{-1} (band I), 1547 cm^{-1} (band II), and 1240 cm^{-1} in the N-doped RGO spectrum are similar to the peaks in the melamine spectrum (see Fig.1F (Curve b)).[54] In addition, the peak (C=O) observed at 1730 cm^{-1} in the GO spectrum almost disappears in the N-doped RGO spectrum (See Fig.1F (Curve c)), indicating the conversion of carboxyl to amide.

These results clearly indicate the covalent bonding of melamine polymer chains to GO via an amide linkage.

Fig. 1

The Raman spectrum of the as prepared (a) GO sheets and (b) nitrogen doped RGO-ZnO nanocomposite (Fig. 2A) displays two prominent peaks at 1340 and 1600 cm^{-1}, which correspond to the well documented D and G band respectively. The intensity ratio of the D and G band is a measure of the disorder, as expressed by the sp^2 /sp^3 carbon ratio. The G band is related to the in-plane bond-stretching motion of pairs of sp^2-C atoms. The D band ("disordered" band) is the breathing mode of the sp^2-rings of the graphene layer that is related to a series of defects: bond-angle disorder, bond-length disorder, and hybridization which are caused by heteroatom (nitrogen/oxygen) doping and structure defects by plasma treatment. Therefore, the relatively increased intensity of the D band for N-graphene indicates that the content of disordered carbon increases after plasma treatment, mainly by nitrogen doping. Fig. 2B shows the XRD patterns conducted in order to investigate the phase and structure of the obtained samples; the XRD patterns for the ZnO and N-doped RGO nanocomposite samples were both recorded. The characteristic ZnO diffractions of (1 0 0), (0 0 2), (1 0 1), (1 0 2), (1 1 0), (1 0 3) and (2 0 0) appear at 31.9°, 34.6°, 36.4°, 47.7°, 56.7°, 63.1° and 66.6° (2θ), respectively (JCPDS file no. 36-1451). In addition, Fig. 2B shows a GO diffraction peak at 23.29°, attributed to the short-range order in the stacked graphene sheets. On the other hand, the XRD pattern of the N-doped RGO-ZnO nanocomposite does not show any diffraction peak in the low angle region as observed in the case of GO XRD, suggesting the reduction of GO during the reaction process. It is suggested that these residual oxygenated functional groups act to encourage intercalation and adsorption of Zn^{2+} ions onto the RGO. The relatively sharp peaks that appear at 2θ around 268, 438 and 528 in

the N-doped RGO-ZnO nanocomposite XRD pattern correspond to the (111), (220), and (311) reflections of ZnO, respectively, in Fig. 2B.[57] The Scherrer formula is used to calculate the nanoparticle size which is 1-10 nm. The peak positions and relative intensities correspond well with the standard XRD data for ZnO (JCPDS card, file No. 36-1451). The results are in good agreement with the TEM data, as discussed below.

Fig. 2

EIS can be employed to investigate the changes in impedance at electrode surfaces as a consequence of the modification process making this a useful tool for testing the kinetic barrier at the electrode interface. Fig. 2C shows the Nyquist diagrams of the freshly polished (a) bare Au electrode, (b) nitrogen doped RGO modified Au electrode, (c) RGO modified Au electrode, (d) nitrogen doped RGO-ZnO nanocomposite modified Au electrode in the presence of light with equimolar $[Fe(CN)_6]^{3-/4-}$. The semicircular part at high frequencies corresponds to the electron transfer limited process, and the linear part at low frequencies corresponds to the diffusion process. A semicircular arc and a straight line can be observed. In a Randle's circuit, it is assumed that the resistance to charge transfer (R_{et}) and the diffusion impedance (W) are both in parallel to the double-layer capacitance (C_{dl}). This parallel combination of R_{et} and C_{dl} with the charge transfer resistance (R_{et}) occurs at the contact interface between the electrode and electrolyte solution. As can be seen in Fig. 2C, the charge-transfer resistance (R_{et}) for $Fe(CN)_6^{3-/4-}$ at the freshly polished (a) bare Au electrode is about 1250 Ω. Fig. 2C (b) shows the N-doped RGO modified Au electrode. The modification of the N-doped RGO on the Au electrode surface could hindrance the interfacial charge transfer and increases the R_{et} to about 1600 Ω. After the Au electrode was coated with the N-doped RGO-ZnO nanocomposite, the impedance decreased, showing a smaller R_{et} (540 Ω). It should be noted that the N-doped RGO-ZnO nanocomposite

has a smaller R_{et} (540 Ω) than the N-doped RGO modified Au electrode or bare Au electrode, which indicates that the incorporation of ZnO improves the charge transfer performance. Fig. 2D displays the Nyquist diagrams of the freshly polished (a) N-doped RGO-ZnO nanocomposite modified Au electrode and (b) nitrogen doped RGO nanocomposite modified Au electrode in the absence of light with equimolar $[Fe(CN)_6]^{3-/4-}$. The N-doped RGO nanocomposite on the Au electrode possess an electron transfer resistance of R_{et} to 2420 Ω (Fig. 2D, curve b). The poor electron conductivity of the N-doped RGO nanocomposite on the Au electrode under absence of light condition leads to an increase in the charge transfer resistance. However, after the Au electrode surface was modified by coating it with the N-doped RGO-ZnO nanocomposite, there is a decrease in the value of R_{et} to 1948Ω (Fig. 2D, curve a) due to reduced negative charge on the surface. The results suggest that the amino type N atoms plays a major role in the high electrocatalytic efficiency due to the large surface area of the ZnO nanoparticles and also the presence of N groups at the RGO surface.As can be seen from the experiment in the presence of light, the electrochemical activity of the N-doped RGO-ZnO modified Au electrode (R_{et} = 540 Ω; curve a in Fig. 2B) exhibits lower R_{et} values than in the absence of light (R_{et} = 1948Ω; curve a in Fig. 2D). This may arise due to the electrostatic interaction between the positive charged N-doped RGO-ZnO modified Au electrode and the negative charged $[Fe(CN)_6]^{3-/4-}$ facilitates electron transport between the interphase, which is expected that the R_{et} would decrease instead of increase. The deposition of ZnO and presence of light acts as a barrier leading to decreased diffusion at the redox probe $[Fe(CN)_6]^{3-/4-}$ for the N-doped RGO-ZnO modified Au electrode.

3.3. Morphology and elemental composition analysis

The surface morphologies of the RGO and N-doped RGO-ZnO nanocomposites can be understood by SEM imaging, as shown in Fig. S1A. The many folds and wrinkles in the RGO

sheets on the ITO surface can be clearly seen. The EDX spectrum shows peaks corresponding to C, and O; see Fig. S1B. Fig. S2A clearly illustrates the morphology of the N-doped RGO-ZnO nanocomposites. The ZnO particles decorating the surfaces and interlayered N-doped RGO sheets can be attributed to the presence of nitrogen containing functional groups and high specific surface are of the RGO surface, which favor the adsorption of ZnO. Further removal of some oxygen-containing groups from the RGO surface leads to a remarkable increase in ZnO particle size due to aggregation, which indicates that the oxygen-containing groups on the N-doped RGO surfaces do play an important role in enhancing the loading of ZnO. Melamine can effectively promote ZnO growth on graphene sheets as can be seen in Fig. S2A. The elemental composition of the N-doped RGO-ZnO nanocomposite was determined using EDX. The EDX results (Fig. S2B) confirmed the existence of C, N, Zn and O, which is consistent with ZnO being present in the N-doped RGO nanocomposite and this result is in a good agreement with the XRD results.

Fig. 3

The morphologies of N-doped RGO sheets and N-doped RGO-ZnO nanocomposite were characterized by TEM. Fig. 3A reveals that the N-doped RGO material consists of corrugated and crumpled sheets. Corrugation and scrolling are part of the intrinsic nature of N-doped RGO sheets. Fig. 3B shows exfoliated N-doped RGO sheet decorated with ZnO aggregates with sizes of 1-10 nm. Some of the flower-like ZnO microstructures on the N-doped RGO sheets were fragmented because of the chemical treatment prior to TEM observation. The flower-like ZnO particles are mainly located at the edge of the N-doped RGO sheets, possible as a result of the aggregation of ZnO particles that confined their efficient dispersion on the N-Doped RGO sheets. The broad diffuse rings in the selected area electron diffraction patterns (SAED) show the

small size of the ZnO nanoparticles. Indexing of the SAED pattern shows (1 0 0), (0 0 2), (1 0 1), (1 0 2), (1 1 0), (1 0 3) and (2 0 0) peaks attributed to the hexagonal crystalline phase of ZnO nanoparticles. Fig. 3D shows an HRTEM image of the ZnO fragment marked with a circle in Fig. 3C. Based on the diffraction rings of the N-doped RGO-ZnO nanocomposites (Fig. 3C) and RGO sheets (Fig. 3D), we can calculate the particle size, which is 1-10 nm. Furthermore. This result is in good agreement with the calculated results from XRD.

Fig. 4

3.4. Electrochemical behaviors of HQ and CC using the N-doped RGO-ZnO modified Au electrode

The photo electrochemical behaviors of HQ and CC at the bare Au electrode, N-doped RGO modified Au electrode and N-doped RGO-ZnO modified Au electrode were studied using CV and SWV; 0.05 M PBS (pH7) was used as the supporting electrolyte; see Fig. 4A. The photo electrochemical responses for the 3 electrodes were tested using samples with and without 1×10^{-4} M HQ and1×10^{-4} M CC. As can be seen in Fig. 4A, for the bare Au electrode (curve b), there is a broad anodic peak at 408 mV and two cathodic peaks at 185 mV and 72 mV, corresponding to the oxidation of CC and HQ, respectively. The results shows that the oxidation peaks of HQ and CC at the bare Au electrode is irreversible with sluggish electron transfer kinetics. In contrast, for the N-doped RGO modified Au electrode (curve e), shows a pair of redox peak of HQ appears at 102 mV and 70 mV with a separation (ΔEp) of 26 mV. Similarly pair of redox peaks of CC appears at 319 mV and 286 mV with a separation (ΔEp) of 33 mV.Which indicates that that significant lowering of the HQ and CC oxidation over potential and the occurrence of fast electron-transfer kinetics at the N-doped RGO modified Au electrode. The peak-to-peak separation between the HQ and CC oxidation peaks is about 104 mV in the

light condition. Compared to the bare Au electrode, there is a great increase in the background current, implying a larger surface area in the N-doped RGO film on the Au electrode. There is also a remarkable increase in the anodic peak current at the N-doped RGO. These results indicate accelerated electron transfer at the electrode surface. Fig.S3 and S4 shows that CV of N doped RGO-ZnO modified film in presence of HQ and CC at (a) dark (b) light irradiation. The results shows that in both HQ and CC detection there is a slight potential shift and peak enchancement in light irraditon than the experiment carried out in dark. On the other hands, the enhancement of the photo electrochemical response to HQ and CC can be partly attributed to the degree of electrostatic interaction between the surface of the N-doped RGO-ZnO modified Au electrode and the dihydroxybenzene isomers with different pKa values. Both HQ (pKa = 10.0) and CC (pKa = 9.4) exist in their protonated forms at pH 7.0. There is a greater increase in the fraction of negatively charged HQ over CC at the diffusion layer of the N-doped RGO-ZnO modified Au electrode surface, possibly due to the π-π interactions between the benzene rings in the HQ and CC and graphene layer which contain electron-rich nitrogen atoms and the hydrogen bonds that form between hydroxyls in the HQ and CC molecules and nitrogen atoms within the graphene layers.[58] This resulted in the relatively energetic electron transfer in addition to the preferable HQ structure, which was capable of resonance stabilization of the intermediate redox reaction. Fig.4B shows that CV of N doped RGO-ZnO modified film in presence of HQ and CC at (a) dark (b) light irradiation. The results show that in both HQ and CC detection there is a slight potential shift and peak enhancement in light irradiation than the experiment carried out in dark.

N-doped RGO-ZnO modified Au electrode surface possess a potential difference for CC and HQ for cathodic (ΔEpc) and anodic peak (ΔEpa) was around 20 mV and 21 mV, respectively.Moreover, there was a remarkable enhancement in the peak currents compared to

that of surface of the N-doped RGO modified Au electrode or bare Au electrode. The separation of the oxidation peak current between HQ and CC is about 112 mV, which is significantly higher, and indicative of the occurrence of fast electron-transfer kinetics at the N-doped RGO-ZnO modified Au electrode in the light condition. This may be due to the abundance of electro active and binding sites for immobilization, and the acceleration of the electron transfer of ZnO provided by the N-doped RGO film. This is probably due to the excellent photo electrocatalytic activity of ZnO, which are responsible for the significantly improved photo electrochemical behaviors of HQ and CC at the N-doped RGO-ZnO modified Au electrode. Fig. 4B shows the CVs of the N-doped RGO-ZnO modified Au electrode for 1×10^{-4} HQ and 1×10^{-4} CC, respectively, measured in the dark. There is a 5-fold increase in the observed current response for 1×10^{-4} HQ and 1×10^{-4} CC at the N-doped RGO-ZnO modified Au electrode (compare Fig. 4B, curve a to curve b) depending on the presence or absence of light. The negative shift in the oxidation potentials and improved peak current responses indicate the good catalytic effect of the N-doped RGO-ZnO modified Au electrode toward the oxidation of 1×10^{-4} HQ and 1×10^{-4} CC. Because of the photo electrochemical process, some photo-generated holes in the ZnO are consumed by the oxidation of HQ and CC. Thus, the recombination of photo generated electron/hole pairs is inhibited, resulting in the enhanced photocurrent response. There is a significant lowering of the HQ and CC oxidation over potential and fast electron-transfer kinetics take place at the N-doped RGO-ZnO modified Au electrode.

3.5. The effect of scan rate and influence of the solution pH

Further experiments were performed to study the photoelectrochemical characteristics of the adsorbance of HQ and CC under optimized conditions at the surface of the N-doped RGO-ZnO modified Au electrode under different scan rates. Fig. 5A shows the superposed CVs of HQ and CC (1×10^{-4} M in 0.05 M PBS) obtained using scan rates ranging from 100 to 1000 mV s^{-1}. Both the anodic peak current (i_{pa}) and the cathodic peak current (i_{pc}) are found to be directly proportional to the scan rates (Inset to Fig. 4B). The relations can be calculated with the following equations: I_{pa}/μA [HQ]= -0.1222x - 1.8087, R^2=0.9921, I_{pc}/μA[HQ]= 0.0973+1.1797, R^2=0.999 and I_{pc}/μA [CC] = 0.1611-0.5602, R^2=0.992, I_{pa}/μA [CC]= -0.1476x - 0.541, R^2=0.9926. The results indicate the adsorption-controlled electrode process of HQ and CC at the N-doped RGO-ZnO modified Au electrode. HQ and CC are easily adsorbed onto the surface of the electrode, and there is sufficient time for their oxidation at the modified surface. Therefore, the simulteanous detection of HQ and CC on N-doped RGO-ZnO modified Au electrode are illustrated as follows

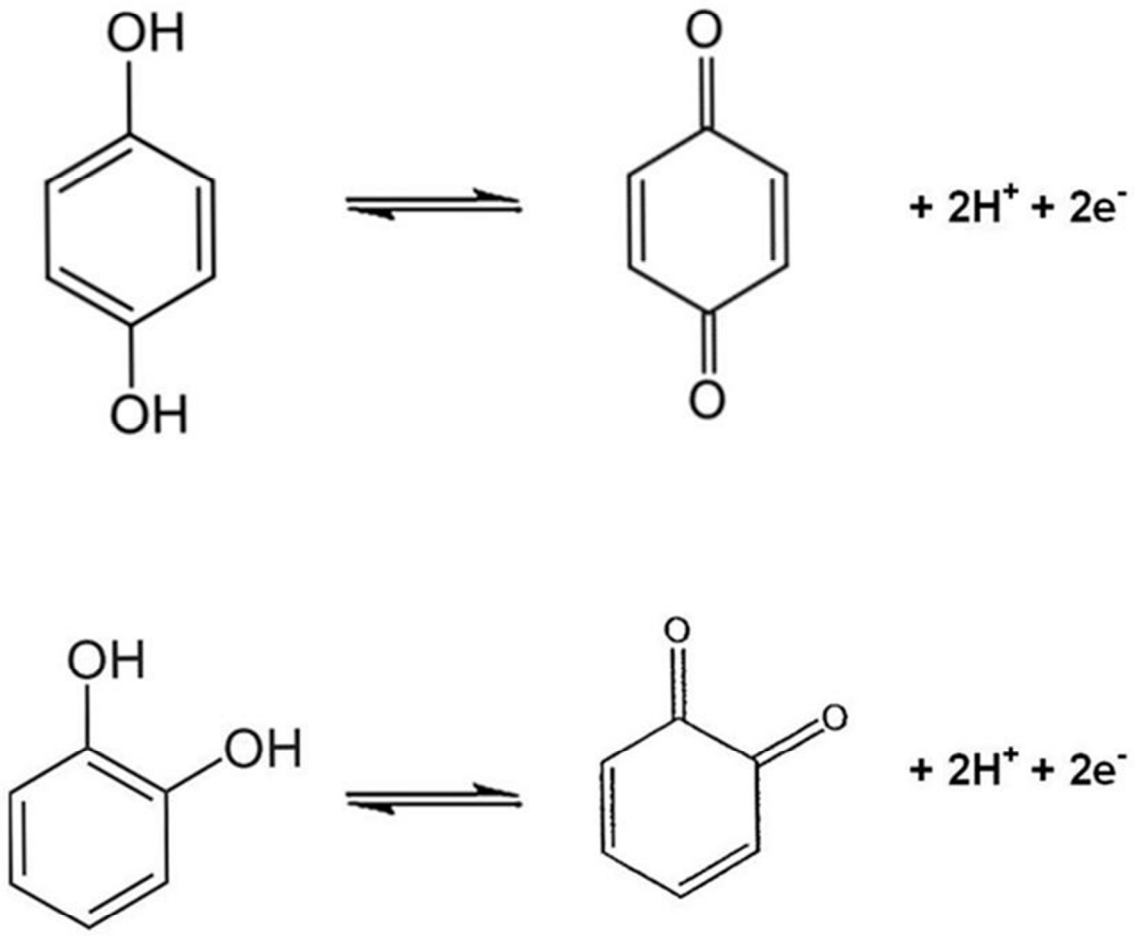

398

399 **Fig. 5.**

400 The effect of pH on the photo electrochemical responses has a significant influence on
401 the oxidations of HQ and CC at N-Doped RGO-ZnO modified Au electrode was studied over the
402 pH ranging from 3.0 to 9.0 with a scan rate of 100 mV s^{-1}. Clearly, one can see from Fig. 5B that
403 the oxidation currents of HQ and CC increase gradually over the pH range from 3.0 to 9.0 and
404 reach a maximum at pH 7, and decrease when the pH value increases gradually. When pH
405 increasing from 3.0 to 7.0, the NH_2 in melamine Doped RGO will be protonated and the

406 hydroxyl in dihydroxybenzenes will not ionized, which will decrease the adsorption capacity of
407 the HQ and CC. When pH is between 7 to 9, the increased hydroxyl ion in solution might also
408 decrease the adsorption capacity of the HQ and CC.

409 On the other hand, as can be seen from Fig. 5B, the oxidation peak potentials of HQ and
410 CC shift negatively along with the increase of pH value. The E_{pa} of HQ and CC shifts to lower
411 potential values as calculated in the following equation: E_{pa}/V = -0.0568-0.6890 pH (correlation
412 coefficient R^2 = 0.9983). The slope of the relation, -57 mV^{-1} pH, which is close to the expected
413 theoretical value of 57.6 mV pH^{-1}. This indicates that the electron transfer number (n) for the
414 oxidation of HQ and CC has been documented to be a two-proton and two-electron process.[59]
415 Considering sensitivity and physiological conditions it was found that the maximum peak current
416 was achieved when 0.05 M PBS was maintained at pH 7. Therefore, pH 7 PBS was selected for
417 the buffer solutions in the experimental work.

418 **3.6. Simultaneous determination of HQ and CC**

419 The main objective of this work was to develop a method capable of separating the
420 electrochemical responses of HQ and CC simultaneously. This was achieved using the N-doped
421 RGO-ZnO modified Au electrode. Under optimized conditions, The SWV results (Fig. 6A) show
422 two well distinguished anodic peaks which correspond to the oxidation of HQ and CC,
423 respectively. A potential difference of 112 mV between the two peak potentials of HQ and CC is
424 large enough to allow simultaneous determination of the concentration. The oxidation peak
425 currents increased with an increase in the mixture concentration and were linear for a wide range
426 of concentrations: 2-300 μM for HQ and 2-250 μM for CC with coefficients of R^2 = 0.9986, and
427 R^2 = 0.9953, respectively and a detection limit of 30 nM. The results show sensitivities of

approximately 67.3 μA mM^{-1} cm^{-2} and 52.5 μA mM^{-1} cm^{-2} for CC and HQ, respectively. The results show that the simultaneous voltammetric determination of HQ and CC in mixed samples was possible with the N-doped RGO-ZnO modified Au electrode, without any cross interferences (Fig.6A). To the best of our knowledge, this is the first time that simultaneous measurement of HQ and CC was successfully achieved with the optimized N-doped RGO-ZnO modified Au electrode.

Fig. 6

3.7. Selective determination of HQ and CC

The excellent electrocatalytic activity of the modified Au electrode also promises selective determination of HQ and CC, when the concentration of one species is changed but the other is kept constant. Examination of the SWV results in Fig. 6B shows that the peak current response for the oxidation of HQ increases linearly with the increase in HQ concentration in the range of (a-g): 2-900 μM. The correlation coefficient of R^2 =0.9945 and the LOD is 10 nM (S/N = 3). Meanwhile, the oxidation peak currents for CC (40μM) remain almost constant, indicating that the addition of HQ does not affect the determination of CC. Similarly, as shown in Fig. 6C, the oxidation peak current of CC increase with an increase in CC concentration while the concentration of HQ (40μM) remained constant. The oxidation peak current is linearly on the concentration of CC in the range between 2-600 μM (R^2 = 0.9962). The LOD is 10 nM (S/N = 3). Fig. 6C shows a linear increase in the oxidation peak current, while the oxidation peak currents for HQ remain almost constant (40μM), which suggests that the presence of HQ did not interfere with the response of CC oxidation. Furthermore, the above measurements results show the sensitivity of the N-doped RGO-ZnO nanocomposite, being 82.82 μA mM^{-1} cm^{-2} for HQ and

63.8 μA mM^{-1} cm^{-2} for CC. All the results strongly suggest that HQ and CC can be separately determined in a mixture using the proposed method. Comparison with past results in the literature suggests that the present sensor is superior to some earlier reported methods, especially for the detection limit and sensitivity; see Table 1. The improved sensitivity can be attributed to the immobilization of the N-doped RGO-ZnO nanocomposite on the Au modified electrode surface which produced a larger surface area, excellent conductivity and good electrocatalytic effect.

3.8. Analytical applications

The practicalability of the proposed modified electrode was also evaluated by testing real samples of skin whitening cream and lake water using the standard addition method with the results being shown in Table 2. Fig. S6 shows the SWV results obtained at N-doped RGO-ZnO nanocomposite modified Au electrode for the simultaneous determination of HQ and CC mixture at similar conditions we use Diluted skin whitening cream and undiluted skin whitening cream samples. During undiluted skin whitening cream samples no peaks were appeared.Meanwhile, when the skin whitening cream (30 mg) was diluted 200 times with 0.05 M pH 7 PBS before measurement. The SWV results on N-doped RGO-ZnO nanocomposite modified Au electrode in Fig. S5 (curve b-f) exhibited two broad peak for HQ and CC mixture appeared. Moreover, the standard addition method was used for testing recovery. The results show that the quantitative recoveries of HQ and CC spiked samples to be 98.6% - 99.5%, 98.6-102.2%, and 99.2-100.8%, 96.4-99.8%. On the other hands, Fig. S7 shows the SWV results obtained at N-doped RGO-ZnO nanocomposite modified Au electrode during the simultaneous determination of HQ and CC mixture at similar conditions we use Diluted lake water and

472 undiluted lake water samples. Undiluted lake water samples there was no peaks appeared in the
473 potential range scanned (curve a). Fig. S7 exhibits the SWV obtained for the different
474 concentrations (curves b-e) of HQ and CC mixture (Diluted lake water solution) at N-doped
475 RGO-ZnO nanocomposite modified Au electrode in the in N_2 saturated PBS. Then, the
476 reproducibility of the method was demonstrated by calculating the mean relative standard
477 deviation (RSD); results are given in Table 2. The results clearly indicate the practical
478 applicability and reliability of the proposed N-doped RGO-ZnO nanocomposite modified Au
479 electrode for simultaneous determination of HQ and CC in water samples.

480 **3.9. Stability**

481 The stability of the N-Doped RGO-ZnO nanocomposite was checked by testing for the
482 presence of HQ and CC in pH 7.0 solutions by successive electrochemical CV scanning for 100
483 cycles. As shown in Fig.S5, there was an obvious decrease in the peak current of HQ and CC
484 with increasing scan cycles. These results indicate that there is an electrochemical interaction
485 between the N-doped RGO-ZnO nanocomposite and the HQ and CC at the surface of the
486 modified electrode. This led to a remarkable acceleration in the rate of electrochemical oxidation
487 of HQ and CC. These results indicate improved film stability. There was no significant change
488 in the response ever after the N-doped RGO-ZnO nanocomposite had been stored at room
489 temperature for at least 20 days. The repeatability of the nanocomposite for simultaneous
490 detection of HQ and CC in a mixture was investigated. The RSD for six successive
491 measurements was 2.03% for CC and 2.15% for HQ. This result shows the good reproducibility
492 of the N-doped RGO-ZnO modified Au electrode. Additionally, a series of five N-doped RGO-
493 ZnO nanocomposite samples were fabricated and tested to obtain RSDs of 3.56% and 4.33% for

CC and HQ, respectively. These results indicate that the N-doped RGO-ZnO nanocomposite had high reproducibility and repeatability.

4. Conclusion

In summary, this work reports on a novel N-doped RGO-ZnO nanocomposite for photoelectrochemical sensing and its application for the simultaneous determination of the oxidation of HQ and CC. An environmentally-friendly, and rapid synthesis methodology was used to synthesize the N-doped RGO-ZnO nanocomposite. The formation of the N-doped RGO-ZnO nanocomposite was confirmed by XRD, and Raman investigation. The N-doped RGO-ZnO modified Au electrode displayed high electrocatalytic activity, and high selectivity and sensitivity for voltammetric measurement of HQ and CC in a mixed solutions, as evidenced by the SWV results. The separation of the oxidation peak potentials for HQ and CC was about 112 mV, respectively, as determined by CV. In addition, the N-doped RGO-ZnO nanocomposite possesses properties such as high sensitivity, low detection limit and wide linear dynamic range. As the electrode fabrication process is very easy and low cost, the present N-doped RGO-ZnO nanocomposite seems to be a good choice for the production of a voltammetric sensor for the simultaneous detection of HQ and CC in biological samples.

Acknowledgements

We wish to express our appreciation to the Ministry of Science and Technology, Taiwan (Republic of China) for support of this work.

References

1. G. Wang, H. Jiao, K. Liu, X. Wu, Y. Dong, Z. Li, C. Zhang, *Electrochem. Commun*., 2014,**41**,47-50.
2. Y. An, L. Tang, X. Jiang, H. Chen, M. Yang, L. Jin, S. Zhang, C. Wang, W. Zhang, *Chem. Eur. J*., 2010,**16,**14439-14446.
3. X. Zhang, S. Li, X. Jin, S. Zhang, *Chem. Commun*., 2011,**47,** 4929-4931.
4. H. Li, J. Li,Q. Xu, X. Hu, *Anal. Chem.,* 2011, **83,** 9681-9686.
5. B. Zhang, L. Lu, Q. Hu, F. Huang, Z. Lin, *Biosens. Bioelectron*, 2014, **56,** 243-249.
6. A. Okamoto, T. Kamei, K. Tanaka, I. Saito, *J. Am. Chem. Soc*., 2004, **126,** 14732-14733.
7. B. Zhang, L. Guo, *Biosens. Bioelectron*, 2012, **37**, 112-115.
8. Z. Yue, W. Zhang, C. Wang, G. Liu, W. Niu, *Mater. Lett*., 2012, **74,**180-182.
9. K. Wang, J. Wu, Q. Liu, Y. Jin, J. Yan, J. Cai, *Anal. Chim. Acta*, 2012, **745,** 131-136.
10. G. Wang, J. Xu, H. Chen, *Sci. China, Ser. B*., 2009, **52,** 1789-1800.
11. W. Lu, Y. Jin, G. Wang, D. Chen, J.H. Li, *Biosens. Bioelectron*, 2008, **23,** 1534-1539.
12. D. Li, M.B. Müller, S. Gilje, R.B. Kaner, G.G. Wallace, *Nat. Nanotechnol*., 2008, **3,**101-105.
13. A.K. Geim, K.S. Novoselov, *Nat. Mater*., 2007, **6,** 183-191.
14. K.S. Novoselov, A.K. Geim, S.V. Morozov, D. Jiang, Y. Zhang, S.V. Dubonos, I.V. Grigorieva, A.A. Firsov, *Science*, 2004, **306,** 666-669.
15. Y. Son, M. L. Cohen, S. G. Louie, *Nature*, 2006, **444,** 347-349.
16. P. Avouris, Z. Chen, V. Perebenios, *Nat. Nanotechnol*. 2007, **2,** 605-615.
17. M. D.Stoller, S.Park, Y.Zhu, J.An, R. Rouff, *Nano Lett*., 2008, **8,** 3498-3502.

18. T.Takamura, K.Endo, L.Fu, Y.Wu, K. J.Lee, T.Matsumoto, *Electrochim. Acta*., 2007, **53,** 1055-1061.

19. Y.Shao, J.Wang, H.Wu, J. Liu, I. A.Aksay, Y.Lin, *Electroanalysis*, 2010, **22,** 1 027-1036.

20. S.Alwarappan, S.Boyapalle, A.Kumar, C.Li, S. Mohapatra, *J. Phys. Chem. C*, 2012 **116,** 6556-6559.

21. Z. Yin, S. Wu, X. Zhou, X. Huang, Q. Zhang, F. Boey, H. Zhang, *small*, 2010, **6,** 307-312.

22. C.Liu, S.Alwarappan, Z. Chen, X. Kong,C. Z. Li, *Biosens. Bioelectron*., 2010, **25,** 1829-1833.

23. J. Hou, Y. Shao, M. W. Ellis, R. B. Moore, B. Yi, *Phys. Chem. Chem. Phys*., 2011, **13** 15384-15402.

24. W.Tu, Y. Dong, J. Lei, H. Ju, *Anal. Chem*., 2010, **82,** 8711-8716.

25. W. Tu, J. Lei, P. Wang, H. Ju, *Chem. Eur. J*., 2011, **17,** 9440-9447.

26. W.W. Zhao, Z.Y. Ma, P.P. Yu, X.Y. Dong, J.J. Xu, H.Y. Chen, *Anal. Chem*., 2012 ,**84,** 917-923.

27. M.H. Asif, S.M.U. Ali, O. Nur, M. Willander, C. Brannmark, P. Stralfors, U.H. Englund, F. Elinder, B. Danielsson, *Biosens. Bioelectron*., 2010, **25,** 2205-2211.

28. S.K. Arya, S. Saha, J.E. Ramirez-Vick, V. Gupta, S. Bhansali, S.P. Singh, *Anal. Chim. Acta*, 2012, **737,** 1-21.

29. C. Klingshirn, *Phys. Status Solidi B*., 2007, **244,** 3027-3073.

30. J. Ding, M. Wang, J. Deng, W. Gao, Z. Yang, C. Ran, X. Zhang, *J. Alloys Compd*., 2014, 82, 29-32.

559 31. Y. Qiu, S. Yang, *Adv. Funct. Mater*., 2007, **17,** 1345-1352.

560 32. J. Wu, X. Shen, L. Jiang, K. Wang, K. Chen, *Appl. Surf. Sci*., 2010, **256,** 2826-2830.

561 33. G. Williams, P.V. Kamat, *Langmuir*, 2009, **25,** 13869-13873.

562 34. B. Li, T. Liu, Y. Wang, Z. Wang, *J. Colloid Interface Sci*., 2012, **377**, 114-121.

563 35. O. Akhavan, E. Ghaderi, R. Rahighi, *ACS Nano*, 2012, **6,** 2904-2916.

564 36. J.Q. Tian, S. Liu, H.Y. Li, L. Wang, Y.W. Zhang, Y.L. Luo, A. Asiri, A.O. Al-Youbi,

565 X.P. Su, *RSC Adv*., 2012, **2,** 1318-1321.

566 37. O. Akhavan, *Carbon*, 2011, **49,** 11-18.

567 38. Y.J. Kim, J.H. Lee, G.C. Yi, *Appl. Phys. Lett*., 2009, **95,** 213101- 213103.

568 39. J. Wu, X. Shen, L. Jiang, K. Wang, K. Chen, *Appl Surf. Sci*., 2010, **256,** 2826-2830.

569 40. T. Lu, Y.P. Zhang, H.B. Li, L.K. Pan, Y.L. Li, Z. Sun, *Electrochim. Acta*, 2010, **55,**

570 4170 -4173.

571 41. B. Li, H. Cao, *J. Mater. Chem*., 2011, **21,** 3346-3349.

572 42. J. Wang, J. Park, X. Wei and C. Lee, *Chem. Commun*., 2003, 628-629.

573 43. H. Truong, S. Lomnicki, B. Dellinger, *Environ. Sci.Technol*., 2010, **44,** 1933-1939.

574 44. J. J. Yu, W. Du, F. Q. Zhao, B. Z. Zeng, *Electrochim. Acta*, 2009, **54,** 984-988.

575 45. Z. H. Wang, S. J. Li and Q. Z. Lv, *Sens. Actuators, B*, 2007, **127,** 420-425.

576 46. H. Chen, J. Yao, F. Wang, M. M. F. Choib, E. Bramanti and G. Zaray, *J. Hazard.*

577 *Mater*., 2009, **167,** 846-851.

578 47. J. A. Zazo, C. B. Casas, A. Molina,J. J. R. *Environ. Sci. Technol*., 2007, **41,** 7164-7170.

579 48. A.J. Saleh Ahammad, Md. Mahbubur Rahmana, G. Xu, S. Kim, J. Lee, *Electrochim.*

580 *Acta* 2011, **56**, 5266-5271.

581 49. H. Du, J. Ye, J. Zhang, X. Huang, C. Yu, J. Anal. Chem., 2011, **650,** 209-213.

582 50. T. C. Canevari, L.T. Arenas, R. Landers, R. Custodio, Y. Gushikem, *Analyst*, 2013, **138,**
583 315-324.
584 51. Y. Kong, X. Chen, C. Yao, M. Ma, Z. Chen. *Anal. Methods*, 2011, **3**, 2121-2126.
585 52. D. Marcano, D. Kosynkin, J. Berlin, A. Sinitskii, Z. Sun, A. Slesarev, L. Alemany, W.
586 Lu, J. Tou, *ACS Nano*, 2010, **4,** 4806-4814.
587 53. X. Zhou, T. Shi, H. Zhou, *Appl. Surf. Sci*., 2012, **258,** 6204-6211.
588 54. D. J. Merline, S. Vukusic, A.A .Abdala, *Polym. J*., 2013, **45**, 413-419.
589 55. D. Graf, F. Molitor, K. Ensslin, C. Stampfer, A. Jungen, C. Hierold, *Nano Lett*. 2007, **7,**
590 238-242.
591 56. O. Akhavan, *ACS Nano*, 2011, **4,** 4174-4180.
592 57. T. Lv, L. Pan, X. Liu, T. Lu, G. Zhu, Z. Sun, *J. Alloys Compd*., 2011**509**, 10086-10091.
593 58. H. Guo, S. Peng, J. Xu, Y. Zhao, X. Kang, *Sens. Actuators, B.*, 2014, **193,** 623-629.
594 59. L.Z. Zheng, L.Y. Xiong, Y.D. Li, J.P. Xu, X.W. Kang, Z.J. Zou, S.M. Yang, J. Xia,
595 *Sens. Actuators.*, *B*., 2013, **177**, 344-349.
596 60. S.J. Li, C. Qian, K. Wang, B.Y. Hua, F.B. Wang, Z.H. Sheng, X.H. Xia, *Sens.*
597 *Actuators, B*., 2012, **174**, 441-448.
598 61. Z.H. Wang, S.J. Li, Q.Z. Lv, *Sens. Actuators.*, *B*., 2007, **127,** 420-425.
599 62. A.J.S. Ahammad, Md.M. Rahman, G.R. Xu, S. Kim, J.J. Lee, *Electrochim. Acta*., 2011,
600 **56,** 5266-5271.
601 63. W.M. Si, W. Lei, Y.H. Zhang, M.Z. Xia, F.Y. Wang, Q.L. Hao, *Electrochim. Acta*,
602 2012, **85,** 295-301.
603 64. L.Y. Chen, Y.H. Tang, K. Wang, C.B. Liu, S.L. Luo, *Electrochem. Commun*. 2011, **13**
604 133-137.

65. T. Gan, J.Y. Sun, K.J. Huang, L. Song, Y.M. Li, *Sens. Actuators., B*., 2013 **177,** 412-418.

66. D.H. Deng, S.J. Li, M.J. Zhang, X.N. Liu, M.M. Zhao, L. Liu, *Anal. Methods*., 2013, **5**, 2536-2542.

67. L.P. Wang, Y. Meng, Q. Chen, J.H. Deng, Y. Zhang, H.T. Li, S.Z. Yao, *Electrochim. Acta*., 2013, **92,** 216-225.

68. S. Hu, Y.H. Wang, X.Z. Wang, L. Xu, J. Xiang, W. Sun, *Sens. Actuators., B*., 2012, **168**, 27-33.

69. Z. Liu, Z. Wang, Y. Cao, Y. Jing, Y. Liu, *Sens. Actuators., B*., 2011, **157**, 540-546.

Figure Captions

Fig.1. XPS spectrum of (A) nitrogen doped RGO-ZnO nanocomposite, (B) C 1s XPS spectra of nitrogen doped RGO-ZnO nanocomposite, (C) deconvoluted O 1s spectra of nitrogen doped RGO-ZnO nanocomposite, (D) N 1s XPS spectra of nitrogen doped RGO-ZnO nanocomposite, (E) Zn 2p core-level spectrum in the nitrogen doped RGO-ZnO nanocomposite, (F) FTIR spectra of GO, melamine and nitrogen doped RGO modified electrodes.

Fig.2. (A) Raman spectra of GO and nitrogen doped RGO-ZnO nanocomposite, (B) XRD patterns of ZnO, and nitrogen doped RGO-ZnO modified electrodes, (C) EIS Nyquist plot for the (a) bare au electrode, (b) nitrogen doped RGO/Au electrode, (c) RGO modified electrode, and (d) nitrogen doped RGO-ZnO modified nanocomposite in presence of light; PBS (pH 7) containing 5 mM $Fe(CN)_6^{3-/4-}$. Inset: Randles equivalent circuit model. (D) EIS Nyquist plot for the (a) nitrogen doped RGO-ZnO nanocomposite, (b) nitrogen doped RGO modified Au electrode in the absence of light; PBS (pH 7) containing 5 mM $Fe(CN)_6^{3-/4-}$.

Fig.3. (A) HRTEM image of nitrogen doped RGO nanocomposite, (B) & (C) HRTEM images of nitrogen doped RGO-ZnO nanocomposites and (D) selected area diffraction pattern (SAED) of ZnO nanoparticles.

Fig.4. (A) CVs recorded at the different modified electrodes in the presence of light with the presence/absence of 1×10^{-4} M HQ and 1×10^{-4} M CC in 0.05 M nitrogen-saturated PBS (pH 7) at a scan rate 50 mV s^{-1}: (a) and (b) bare Au electrode, (c) and (e) nitrogen doped RGO, (d) and (f) nitrogen doped RGO-ZnO modified Au electrode (B) CVs of (a) & (b) nitrogen doped RGO-

651 ZnO modified Au electrodes in presence/absence of light of 1×10^{-4} M HQ and 1×10^{-4} M CC in
652 0.05 M nitrogen-saturated PBS (pH 7) at a scan rate 50 mV s^{-1}.
653
654 **Fig.5.** (A) CVs of nitrogen doped RGO-ZnO modified Au electrode with 1×10^{-4} M HQ and $1 \times$
655 10^{-4} M CC in 0.05 M deoxygenated phosphate buffer solution (pH7) at different scan rates: 0.1,
656 1.0 V s^{-1}. Inset: Plot of I_{pa} and I_{pc} versus scan rates. I_p/μA is presented as a function of v/(Vs^{-1}),
657 I_{pa}/μA [HQ]= -0.1222x - 1.8087, R^2=0.9921, I_{pc}/μA[HQ]= 0.0973+1.1797, R^2=0.9999 and I_{pc}/μA
658 [CC] = 0.1611-0.5602, R^2=0.992, I_{pa}/μA [CC]= -0.1476x - 0.541, R^2=0.9926. The error bars
659 represent the standard deviation after 3 independent measurements. (B) CVs of nitrogen doped
660 RGO-ZnO modified Au electrode with 1×10^{-4} M HQ and 1×10^{-4} M CC in 0.05 M
661 deoxygenated phosphate buffer solutions (pH7) with different pHs: (a-e) 3.0, 5.0, 7.0, 9.0, 11.0.
662 Inset: Effect of pH on anodic peak current and anodic peak potential for CC and HQ.
663
664 **Fig.6.** (A) SWVs of nitrogen doped RGO-ZnO modified Au electrode with various
665 concentrations of CC and HQ in 0.05 M PBS (pH 7) at a scan rate of 0.05 V s^{-1}: (a-h) 2, 48, 80,
666 111, 179, 206, 255, and 300 μM for HQ. Insets show the linear dependence of Ipa of HQ with
667 concentration: (a-h) 2, 32, 70, 120, 160, 190, 210, and 250 μM for CC. Insets show the linear
668 dependence of Ipa of CC with concentration. [B] SWV s of the nitrogen doped RGO-ZnO
669 modified Au electrode in the presence of 40 μM CC with different concentrations of HQ: (a-g) 2,
670 170, 379, 536, 662, 785, and 900 μM. Insets show the calibration plots of HQ and CC. (C)
671 SWVs of the nitrogen doped RGO-ZnO modified Au electrode with 40μM HQ but different
672 concentrations of CC: (a-j) 2, 60, 120, 230, 350, 380, 420, 460, 520, and 600 μM. Insets show
673 the calibration plots of HQ and CC.

674 **Figures**

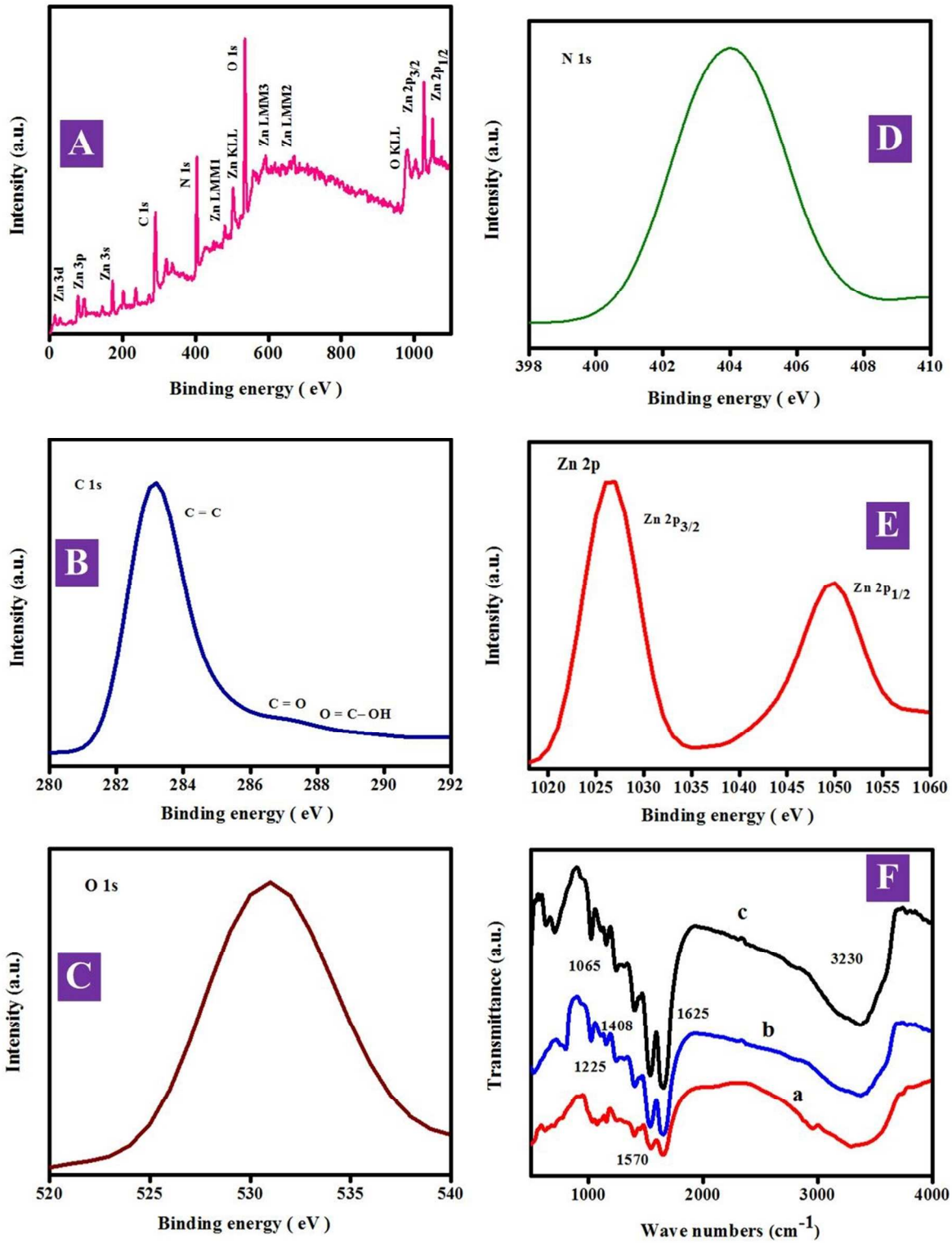

675

676 **Fig. 1**

677

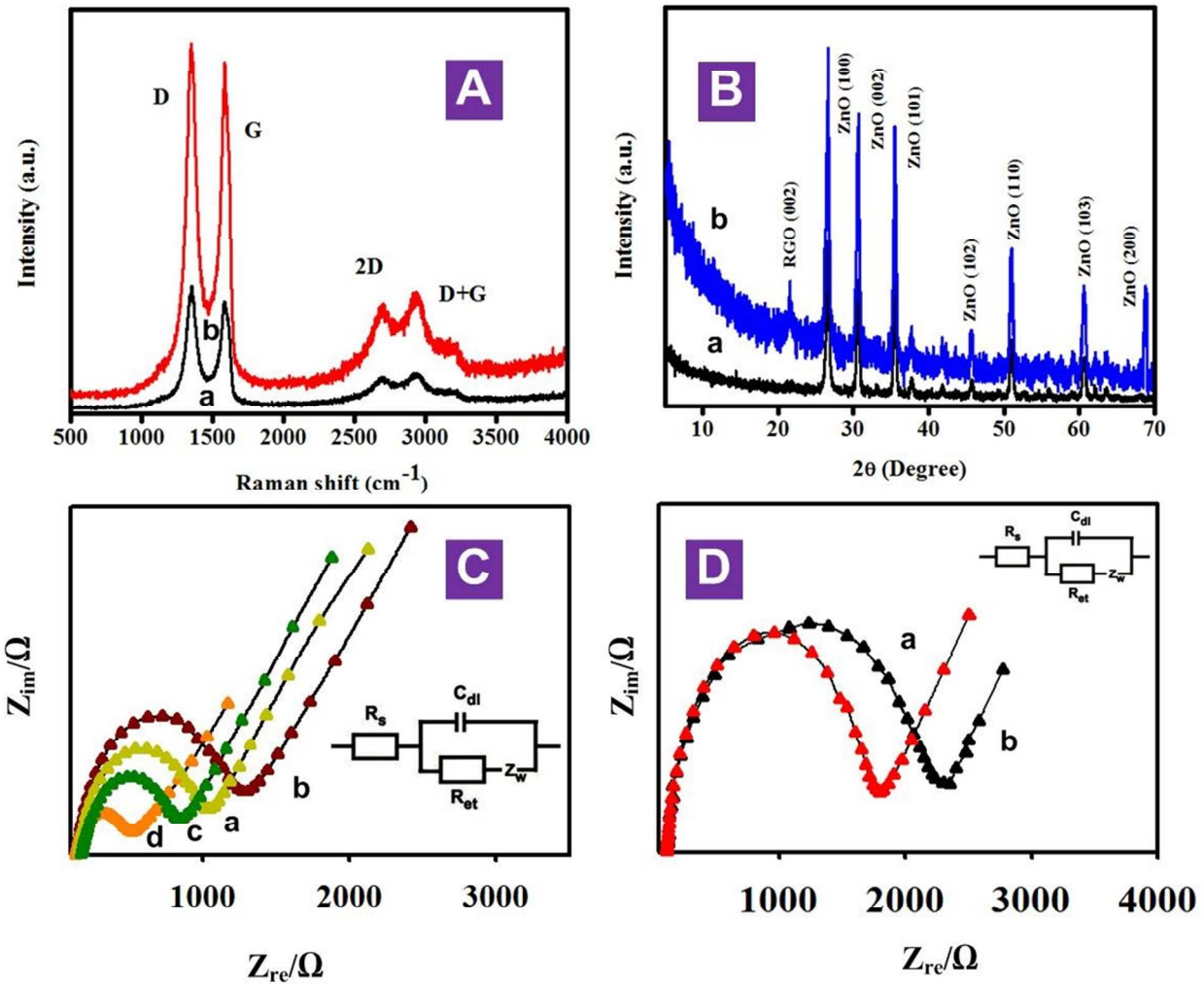

678
679

680 **Fig. 2**

681

682

683

684

685

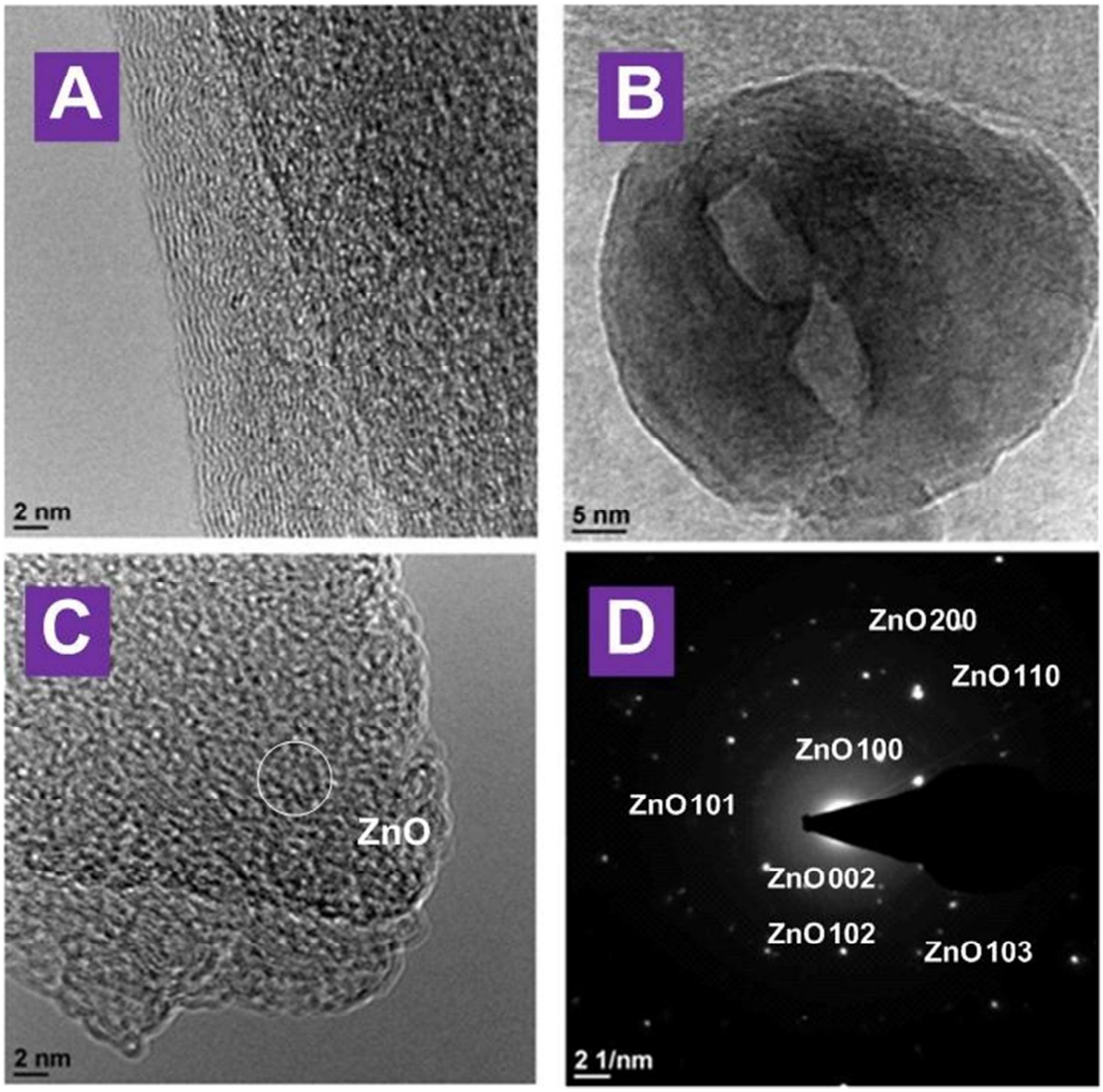

686

687 **Fig. 3**

688

689

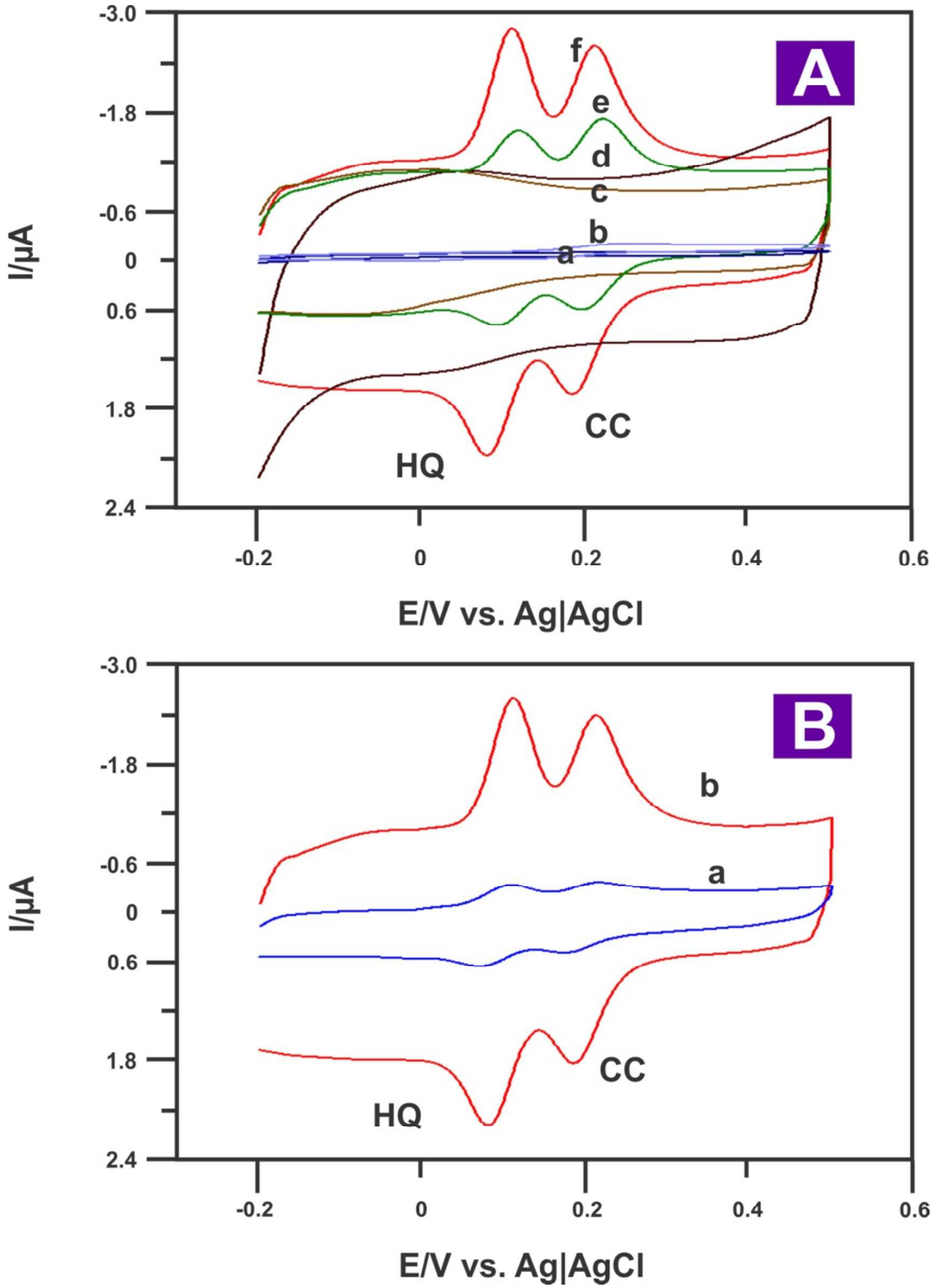

690

691 **Fig. 4**

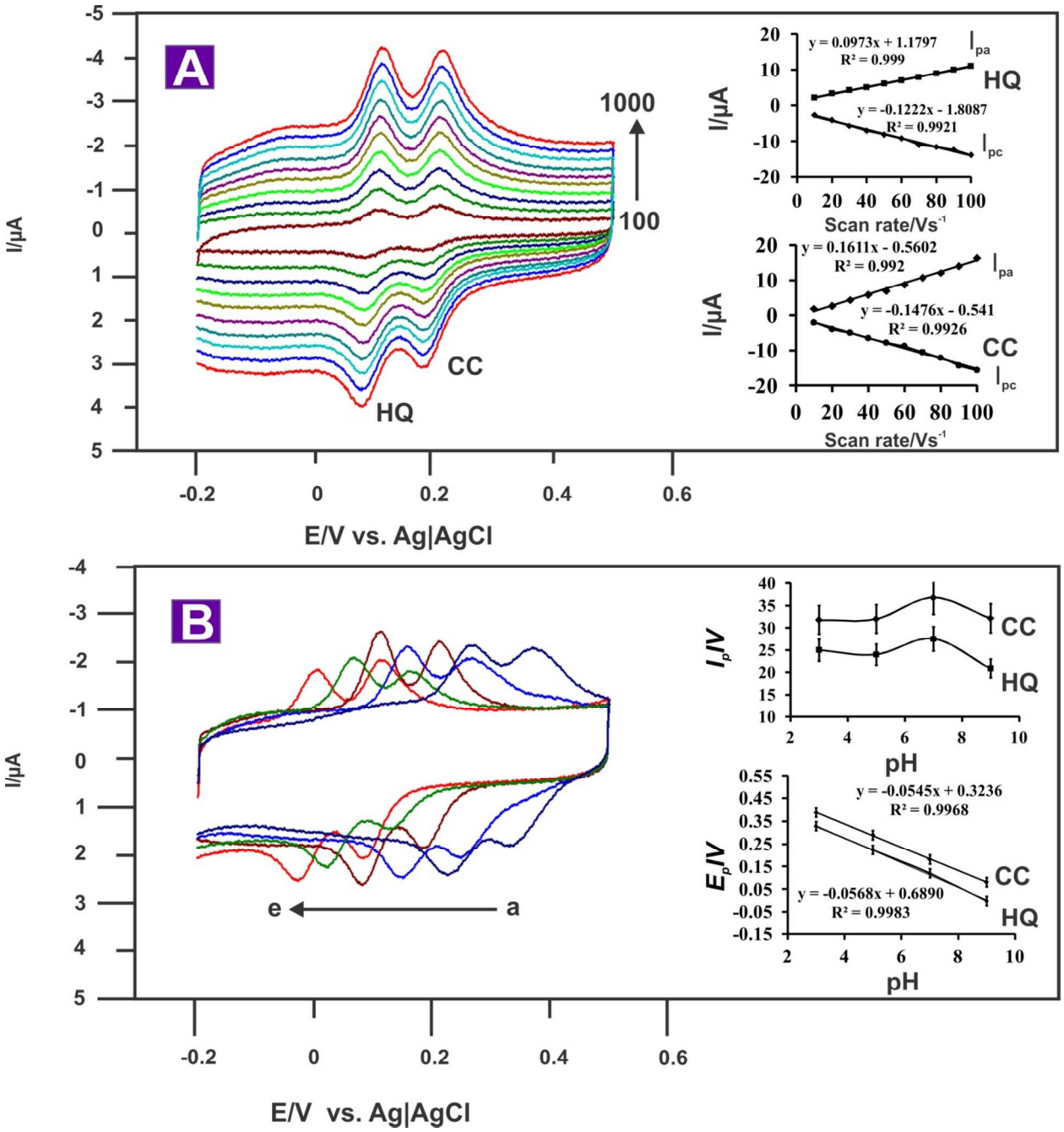

692

693 **Fig. 5**

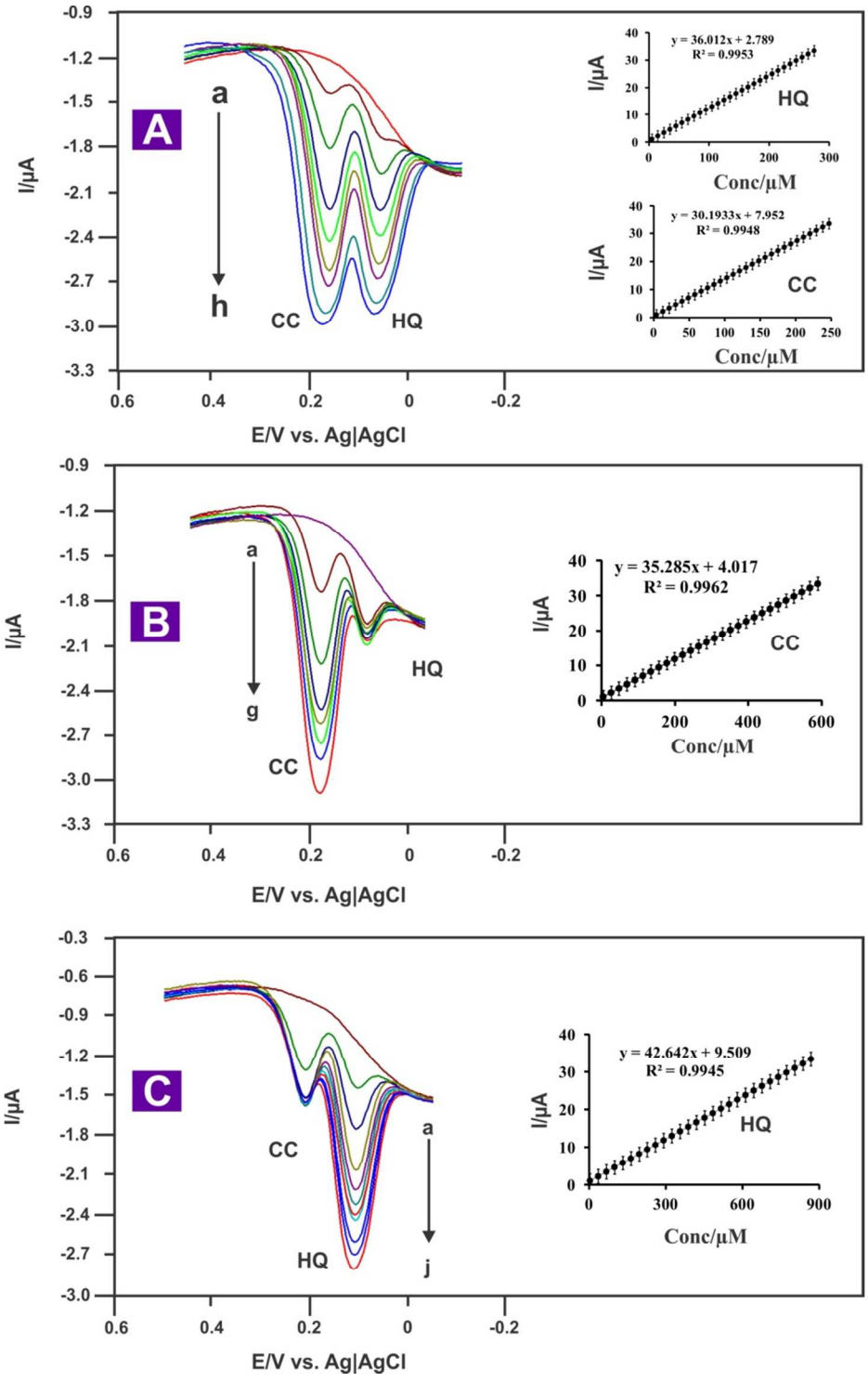

694

695 **Fig. 6**

696

697 **Table 1**

698 **Comparison of the analytical performance of different modified electrodes for**
699 **simultaneous determination of HQ and CC.**

Modified electrode	Analytes	Linear range/μM	Detection limit (nM)	Ref.
Pyridinic nitrogen doped graphene	HQ CC	5-30; 30-200 5-200	380 1000	58
Poly dopamine-reduced graphene oxide	HQ CC	1-230 1-250	720 820	59
Thermally reduced graphene oxide	HQ CC	1-500 1-500	750 800	60
Single-wall carbon nanotube	HQ CC	0.4-10;40-100 0.4-10; 40-100	120 260 300	61
Poly(thionine)	HQ CC	1-120 1-120	30 25	62
Poly(3,4-ethylenedioxy-thiophene)/graphene oxide hybrid film	HQ CC	2.5-200 2-400	1600 1600	63
Electro deposition of reduced	HQ CC	6-200 1-200	200 100	64

graphene oxide				
Graphene oxide-mesoporous MnO_2 nanocomposite	HQ CC	0.01-0.7 0.03-1	7 10	65
Gold nanoparticle/sulfonated graphene nanocomposites	HQ CC	5-100 5-100	1000 2000	66
Nafion-(4-ferrocenylethyne) phenylamine-carbon nanoparticles-graphene	HQ CC	0.3-90 0.6-100	100 200	67
Gold nanoparticle and graphene nanocomposite film co-electrodeposited with carbon ionic liquid	HQ	0.36-800	113	68
Graphene/$BMIMPF_6$nanocomposite	HQ CC	0.5-50 0.5-50	10 20	69
N-Doped RGO/ZnO/Au modified electrode	HQ CC	2-900 2-600	10 10	This work

700

701

702

703

704 Table 2

705 Simultaneous determination results for CC and HQ in samples in skin whitening cream and lake
706 water by the N-doped RGO-ZnO modified electrode.

Sample No	Spiked(μM)		Found(μM)		RSD (%)		Recovery (%)	
	HQ	CC	HQ	CC	HQ	CC	HQ	CC
Diluted skin whitening cream	40	20	39.2	19.6	1.7	2.3	98.6	99.2
	60	40	59.8	39.3	2.7	3.4	99.5	100.8
Diluted lake water	40	20	39.5	19.2	2.5	3.0	98.6	96.4
	60	40	59.2	39.5	2.3	1.4	102.2	99.8

707

708